Enabling Fine-Grain Free 2-Micron Thick CISe/CIGSe Film Fabrication From A Non-Hydrazine Based Solution Processing Route

Swapnil D. Deshmukh, 1 Kyle G. Weideman, 1 Ryan G. Ellis, 1 Kim Kisslinger, 2 Rakesh Agrawal 1*

¹Davidson School of Chemical Engineering, Purdue University, West Lafayette, IN 47907, USA

²Center for Functional Nanomaterials, Brookhaven National Laboratory, Upton, NY 11973, USA

Abstract:

Solution processing of CuInSe₂/CuInGaSe₂ (CISe/CIGSe) photovoltaic devices from a non-hydrazine based routes have been studied for the past few years and a significant improvement in device performance has been achieved via multiple solvent routes. However, none of these routes have ever reported the fabrication of absorber with a thickness above 1.2-1.3 micron which is almost half of what has been traditionally used in vacuum based high efficiency CIGSe devices. The main cause behind this limitation is the formation of a fine-grain layer in solution based systems. Here we manipulate the formation of the fine-grain layer in an amine-thiol based solution route through surface modifications at the bottom Mo layer and achieve active area efficiency up to 14.1% for CIGSe device. Further, with a detailed analysis of the fine-grain layer, not just for the amine-thiol based route, but also for the dimethylformamide-thiourea based route we identify the cause behind the formation of such layers as the presence of sulfide material and carbon impurity (if any) in the precursor film. We utilize the amine-thiol solvent system's ability of selenium and metal selenide dissolution to demonstrate the reduction in the formation of sulfide materials and the extent of trapped carbon in the precursor film. With modified precursor films, we then successfully grow CISe/CIGSe thin films of 2-micron thickness with complete absence of fine-grain layer via high temperature, thickness independent bulk growth mechanism. The growth was realized with and without the presence of excess Se vapor during the heat treatment making this film morphology similar to the one fabricated from high efficiency hydrazine based route.

Introduction:

The chalcopyrite CuInGaSe₂ (CIGSe) thin film photovoltaic material has reached lab scale device efficiency of around 23.4%. Such high efficiency device fabrication was enabled by implementing various advances that have been studied in the CIGSe system over the past few years. Some of these advances include optimization of the absorber deposition process, developing bandgap grading in the absorber with the use of gallium composition variation, changing surface properties with surface sulfurization optimization, use of heavy alkali postdeposition treatments, optimizing the buffer layer deposition, etc.^{2,3} While the use of these various approaches indeed realized a high performing CIGSe devices, these absorbers are typically fabricated through vacuum based deposition routes, causing potential limitations for achieving low cost, high throughput uniform module fabrication on a large scale. To overcome these challenges, researchers are working on developing a solution processing route with high device performance. Currently, the hydrazine based CIGSe thin film deposition route holds the record for the highest efficiency of a solution based CIGSe PV device with a reported value of 18.1%. However, due to the toxicity and explosive nature of the hydrazine solvent system, other nonhydrazine solution processing routes are being studied for the deposition of CIGSe thin films. For this, the two main methods involve the use of nanoparticles⁵ and molecular precursor solutions.⁶ Amongst different successful molecular precursor approaches, some use protic solvents like water, alcohols, amines, thiols while other use aprotic solvents like dimethyl sulfoxide (DMSO) and dimethyl formamide (DMF).7 Currently, the aminethiol solvent system has produced the highest efficiency nonhydrazine based solution processed device with an active area efficiency of 16.4% for CIGSe thin films. 8 This solution system has also successfully demonstrated gallium grading, silver addition, 10 and surface treatments like sulfurization 11 and creating ordered vacancy compounds⁸ for improvement of uniform CIGSe thin films through solution processing routes. Other than aminethiol, routes which have produced CIGSe devices with efficiency

around 14-15% involve CuInGaS₂ (CIGS) nanoparticles, ¹² alcohol based route, ¹³ and DMF-thiourea based route. ^{14,15}

While different solution processing routes are constantly improving the PV performance of CIGSe devices, one major difference in these devices compared to high efficiency vacuum based CIGSe films is the absorber thickness. All non hydrazine solution processed films reported till date have fabricated absorber layer up to maximum of 1.2-1.3 µm thickness, which is almost half of what has been used in vacuum based films. The current highest efficiency amine-thiol device has the absorber thickness of only 900 nm with almost 400 nm thick uncoarsened fine-grain layer sitting under the absorber grains.⁸ In most routes the formation of this layer is associated with the presence of impurities in the film prior to high temperature annealing which tend to get accumulated as a separate layer. Presence of such layer and also particularly its position in the film morphology could drastically affect the film performance. As mentioned earlier, while this layer limits the thickness of the absorber material which affects both the light absorption and carrier collection, it also reduces the control over absorber composition due to non-uniform elemental distribution between these layers.

In this work, we control the morphology of CuInSe₂ (CISe)/CIGSe thin films fabricated from the amine-thiol solvent system by manipulating the solution composition and substrate selection. Fabrication of the absorber material on thin MoO₃ layer instead of directly on Mo leads to improvements in device performance by altering the position of fine-grain layer in the film architecture. This allows us to fabricate a CIGSe thin film having uniform composition with active area efficiency of 14.1%, almost 1-2% higher than previously reported amine-thiol based uniform CIGSe films. Analysis of the fine-grain layer further provides insights into traditional growth mechanism and possible cause for its formation in the film morphology, not just in the case of the amine-thiol route, but for routes that rely on selenization of sulfide precursor films. By utilizing amine-thiol solution's ability to dissolve selenium and metal selenide precursors, film

compositions are altered and their effect on contaminant concentration in the precursor film as well as the grain growth is studied systematically with the help of Raman spectroscopy, scanning electron microscopy, and energy-dispersive X-ray spectroscopy analysis. With this analysis and optimization, we demonstrate the fabrication of impurity free precursor films which are qualitatively identical to hydrazine based films. This allows us to fabricate the first ever hydrazine-free 2-micron thick CISe/CIGSe absorber layer, free of any fine-grain material from a hydrazine-free solution processing route. The modified growth mechanism leading to such morphology however changes the electronic properties of the film and more work is underway to understand the changes in optoelectronic properties to utilize this solution route for high efficiency, large scale film fabrication.

Experimental Section:

Materials:

In powder (99.999%) was purchased from STREM. Ga pellets (99.9999%) and In₂Se₃ (99.99%) were purchased from Alfa Aesar. Cu₂S (99.99%), Se (99.99%), Cu₂Se (99.95%), CuCl (99.995%), InCl₃ (99.999%), Thiourea (TU, >99%), Butylamine (BA, 99%), 1,2-ethanedithiol (EDT, >98%), N, N-dimethylformamide (DMF, 99.8%), and Acetonitrile (99.8%) were purchased from Sigma-Aldrich. All chemicals were used as received except for Ga pellets, which are scraped with a razor blade to remove a possible oxide layer on the surface prior to dissolution.

Ink Formulations

Amine-thiol based inks for CuInS₂ (CIS) and CIGS precursor film fabrication were prepared in BA using stoichiometric additions of thiol. First In or In+Ga were dissolved in BA-EDT solution with EDT:In or EDT:(In+Ga) ratio of 2. After complete dissolution, Cu₂S powder was added to this solution along with some more EDT such that EDT:Cu of 1. This BA based ink was used for coating films for device fabrication. For FTIR studies, some inks were prepared in acetonitrile solvent where the EDT:metal ratio was kept constant but the quantity of BA was reduced to BA:EDT of 2 instead of using BA as a bulk solvent in excess.

Selenium containing inks were prepared by adding required quantities of elemental Se in CIS/CIGS BA-EDT ink. For metal selenide inks, Cu₂Se, In₂Se₃, and elemental Se were added together to BA-EDT solutions to get indium concentration of 0.2 M, Cu:In of 0.9, and EDT:(Cu+In) of 3. DMF based inks were prepared by dissolving 2.28 M thiourea in DMF solvent. After complete dissolution, InCl₃ was added to this solution and stirred overnight to get a 0.4 M indium concentration. CuCl was then added to this solution to get Cu:In ratio of 0.9. Hydrazine based ink was prepared by codissolving Cu₂S, In₂Se₃, S and Se at room temperature with Cu/In ratio of 0.9.

Film and Device Fabrication

CIS/CIGS precursor film was fabricated by blade coating onto 2" \times 1" molybdenum coated (\sim 800 nm) soda lime glass substrate using the BA-EDT ink mentioned above. Multiple layers of this ink were coated to get the desired thickness of the film. This coating was performed via bar coating technique using a auto blade coater with a glass rod. The coating speed was around 20 mm/s with 2 back and forth passes per layer. After each

coating, the film was immediately annealed on a pre-heated hot plate between 300-350 °C for 2-5 min. 10-15 nm of sodium fluoride was then deposited on top of the as-prepared precursor film by electron-beam deposition. The film was then selenized by exposing it to Se vapor in a non-pyrolytic graphite box (containing the sample and elemental Se pellets) at 500 °C for 25 min in a preheated tube furnace. Photovoltaic devices were completed by chemical bath deposition of \sim 50 nm cadmium sulfide (CdS), sputtering of \sim 80 nm intrinsic zinc oxide (ZnO) followed by \sim 220 nm indium tin oxide (ITO), and electron-beam deposition of 100 nm Ni/ 1000 nm Al grids. Each device on the film was separated by mechanically scribing, defining a total area of \sim 0.47 cm2. For MoO3 deposition, thermal evaporation apparatus was used and 5-10 nm of MoO3 was deposited on 2"x1" molybdenum coated glass substrate.

Exfoliated films were prepared by separating the films from the molybdenum substrate. This was done by gluing a sheet of 1.8mm soda lime glass to the CISe film surface with a quick setting two-part epoxy (Loctite, EA 9017) and mechanically separating the SLG support and the SLG/Mo substrate, exposing a clean, flat interface.

Characterization

X-ray diffractograms (XRD) were obtained using a Rigaku Smart Lab diffractometer in Parallel-Beam mode, using a Cu K α ($\lambda = 1.5406$ Å) source operating at 40 kV/44 mA. STEM-EDS data were collected on Talos 200X TEM containing four silicon drift detectors using a SiN grid. Raman and Photoluminescence spectra were collected on a Horiba/Jobin-Yvon HR800 microscope with an excitation laser wavelength of 632.8 nm. FTIR spectra were collected on Thermo-Nicolet Nexus 670 FTIR unit in transmission mode using NaCl crystal substrates. The bulk composition was analyzed using a Fisher XAN 250 X-ray fluorescence (XRF) instrument at 50 kV voltage with a primary Ni filter containing a silicon drift detector. A FEI Quanta 3D FEG Dual-beam SEM was used to obtain the micrographs of the films. The J-V characteristics were measured with a four-point probe station using a Keithley 2400 series source meter while the sample rested on a temperature-controlled stage at 25 °C. Illumination was provided by a Newport Oriel solar simulator with an AM1.5 filter set and calibrated to 1 sun intensity using a Si reference cell certified by NIST.

Result and Discussion:

Location of Fine-grain Layer

To create an ink suitable for scalable film fabrication, stoichiometric quantities of amine and thiol were used for dissolution of metal precursors (Cu₂S, In and Ga) to avoid the presence of any unreacted excess amine and thiol in the solution. Inks obtained with this dissolution were then used to fabricate precursor thin films of sulfide material by blade coating the solution on a glass substrate. Coated liquid films were then annealed in an inert nitrogen atmosphere at different temperatures to study the removal of organic solvents. FTIR data collected on these films show complete removal of organic residue (i.e. C-H stretch) for temperature of 350 °C (Figure 1). To verify whether the solvent used for film fabrication plays any role in determining minimum temperature for removal of organic residue from the film, two different solvents, butylamine and acetonitrile were used for film fabrication. However, both the solvents showed

identical results suggesting that the metal thiolates formed in the solution are primary source of organic residue in the film.

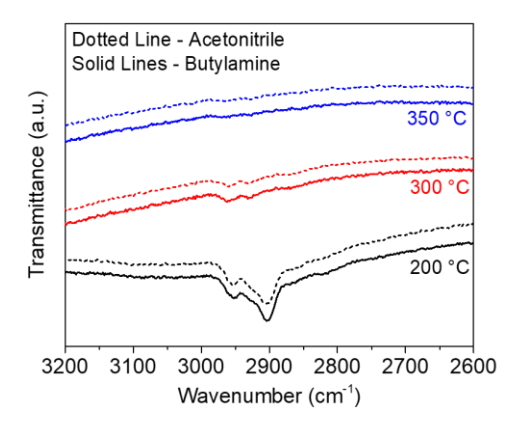


Figure 1. FTIR data collected on CIS films coated with two different solvents; Acetonitrile and Butylamine, annealed at different temperatures

After identifying the minimum temperature required for removal of organic residue, CIS films of around 1-micron thickness were fabricated on Mo coated SLG substrate and selenized in a tube furnace at 500 °C for 25 min under selenium atmosphere. XRD and Raman spectra on this film confirm the formation of chalcopyrite CISe phase with an absence of any secondary material (Figure S1). However, the SEM cross-section shows the formation of trilayer morphology with a fine-grain layer sandwiched between two CISe grain layers (Figure 2a). This observation is consistent for gallium containing films, i.e. selenized CIGS precursor films (Figure S2). Traditionally, CIGS nanoparticle films have been shown to grow from the top surface giving a bilayer morphology with larger grains at the top and a fine-grain layer at the Mo interface. 12,16,17 While the films from DMF/DMSO-TU based routes and previous amine-thiol based routes have shown to grow from both top and bottom giving 2 grain morphology. 14,18,19 The reason for the difference in grain growth between two different routes could be related to the solvents used for film fabrication or the extent of organic residue remaining in the film prior to selenization which could affect the nucleation from the Mo interface. For the case where grains are growing from the bottom, the Mo surface must be acting as a nucleation center for CISe grains. To understand the role of the substrate, a CIS film was deposited directly on soda-lime glass and selenized under similar conditions. As can be seen from Figure 2b, the selenized film shows grain formation only from the top surface with a fine-grain layer near the glass interface. This confirms that the Mo interface indeed serves as a nucleation site for CISe grains.

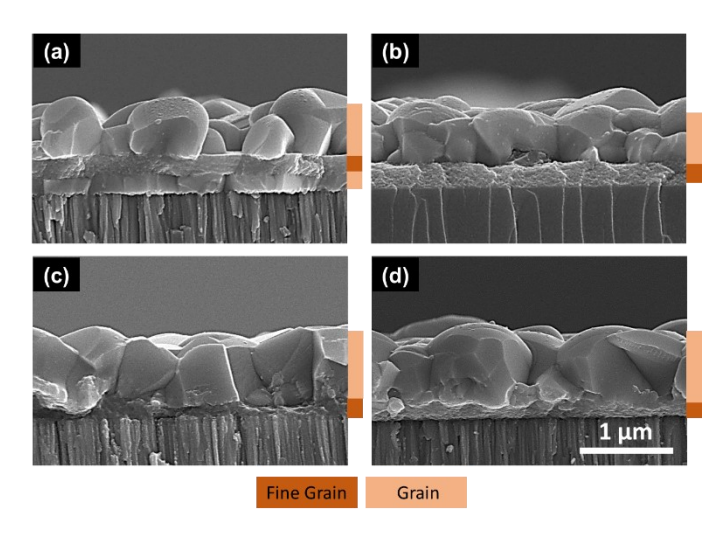


Figure 2. Cross-section SEM images of selenized CIS film coated (a) on Molybdenum, (b) directly on soda lime glass, (c) on 10 nm MoO3 coated Molybdenum, and (d) on 5 nm MoO3 coated Molybdenum

A similar phenomenon was observed in literature for Cu₂ZnSnSe₄ (CZTSe) thin films fabricated via selenization of sulfide Cu₂ZnSnS₄ (CZTS) films. A film deposited on Mo substrate grew as 2 layers of grains while the one deposited on glass grew into single grain morphology. Other similar studies suggest the use of a thin layer of SiO₂, TiN, MoO₃ on the Mo surface to change the interface between precursor material and back contact. Ohile no such surface modifications for changing grain morphology were studied in the case of CISe/CIGSe thin films, one study showed that a thin layer of MoO₃ layer between CIGSe absorber and Mo back contact improves the band alignment of CIGSe devices.

To study the effect of surface modification on grain morphology and device performance, 10 nm of MoO₃ was deposited on the Mo surface via thermal evaporation at the rate of 0.02-0.03 nm/s. A CIS film was then coated on this modified substrate and selenized under similar conditions. As can be seen from Figure 2c, the addition of the MoO₃ layer indeed avoided the growth of CISe grains from the Mo interface and resulted in bilayer instead of trilayer morphology. A similar result was obtained when the MoO₃ film thickness was reduced to as low as 5 nm (Figure 2d). When devices were fabricated from films of around 1-micron thickness with and without MoO3 layer, an absolute improvement of 2.3% was observed in power conversion efficiency for devices containing MoO₃ layer (Table 1). JV data collected on these devices shown in Figure 3 suggest that the improvement was not necessarily observed in the current generation or the open-circuit voltage, rather it was observed in the fill factor of the device (from 50.3% to 65.4%) by reducing the series resistance and increasing the shunt resistance of the device. This confirms the effect of interface modifications on the performance of the device and the need for avoiding a trilayer growth.

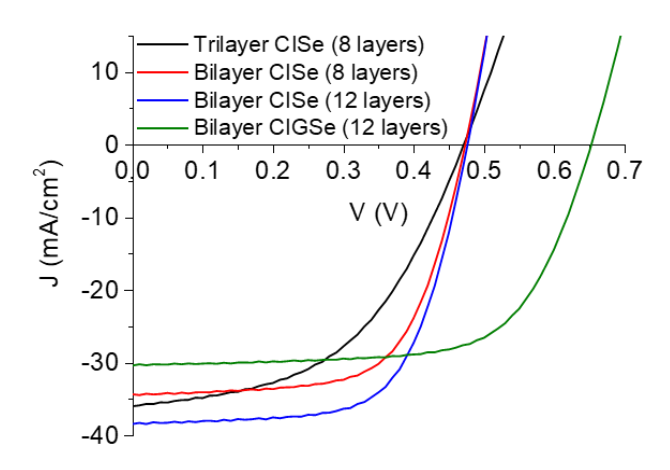


Figure 3. JV characteristics of selenized CIS and CIGS film with different film morphologies

With the modification near the back contact of the film, device optimization was performed by increasing the thickness of CIS precursor film and by introducing gallium in the film. Performance of the devices fabricated is shown in Table 1 which highlights the improvement in efficiency through increased Jsc for a film with higher thickness and a further increase in efficiency through increased Voc for a film with the addition of gallium. The active area efficiency of 14.1% observed here for CIGSe device is the highest for amine-thiol based uniform composition CIGSe films. The application of a gallium gradient, surface treatments, OVC near interface, Ag addition, and heavy alkali treatments are known to improve the performance of CIGSe films, where a number of the aforementioned techiques have already been demonstrated for amine-thiol based route, 8-11 our amine-thiol based uniform CIGSe film has more potential to improve its performance through these modifications.

Table 1. JV parameters for CISe and CIGSe devices prepared from selenization of CIS and CIGS precursor films

	Π (Π _{Active}) (%)	Jsc (mA/cm ²)	Voc (mV)	FF (%)	Rs (Ω.cm ²)	Rsh (Ω.cm ²)
A	8.5 (8.9)	35.9	470	50.3	2.72	244
В	10.8 (11.3)	34.6	480	65.4	1.26	786
C	12.2 (12.8)	38.5	480	66.2	1.15	1379
D	13.4 (14.1)	30.0	650	68.6	1.24	1176

(A=Trilayer CISe with 8 layers and no MoO₃, B=Bilayer CISe with 8 layers and 10 nm MoO₃, C=Bilayer CISe with 12 layers and 10 nm MoO₃, D=Bilayer CIGSe with 12 layers and 10 nm MoO₃)

Analysis of Fine-grain Layer

Although a promising efficiency has been achieved with amine-thiol CISe/CIGSe films by manipulating the location of the fine-grain layer, the presence of the fine-grain layer isn't ideal and has limited the absorber thickness to a maximum of around 1.2-1.3 µm for the current highest efficiency solution processed routes. This thickness is almost half of what has been traditionally used in high efficiency vacuum based routes. To understand the cause of fine-grain layer formation in amine-thiol based film, the layer was analyzed using Raman spectroscopy. However, as this technique uses a 632.8 nm laser, it doesn't penetrate to the back of a 1-micron thick film and hence gives a signal primarily corresponding to the top of the film which generally doesn't have

a fine-grain layer. To access the fine-grain layer for Raman spectroscopy analysis, the film was exfoliated using epoxy and then the analysis was performed from the back surface. The Raman spectrum obtained from the back of the film shows a small peak corresponding to CISe at ~178 cm⁻¹ which is believed to be representing the bottom of the CISe grain (Figure 4a). However, it shows a very strong peak corresponding to amorphous selenium near 250 cm⁻¹ and a characteristic peak corresponding to graphitic carbon in the range of 1300-1600 cm⁻¹ suggesting a presence of C and Se in this layer (Figure 4b).^{25–27} As no organic species is introduced in the film during selenization, the source of graphitic carbon in selenized film must be originating from the precursor film itself. While FTIR study of the precursor film did not show any organic carbon residue for a film annealed at a temperature of 350 °C, Raman spectroscopy on the same precursor film confirmed the presence of graphitic carbon prior to selenization (Figure S4). In previous work, it was shown that copper and indium form metal thiolate species when dissolved in amine-thiol solution.²⁸ The thiol in these thiolates serves as a sulfur source for metal sulfide material. In this reaction when metal sulfur bond is formed from a thiolate species, a C-S bond is broken and if both the C-S bonds break from a dithiol molecule the carbon could get converted to graphitic carbon during annealing and may not leave easily from the film. This carbon can remain in the film during selenization giving rise to a fine-grain layer and hence needs to be removed completely prior to selenization.

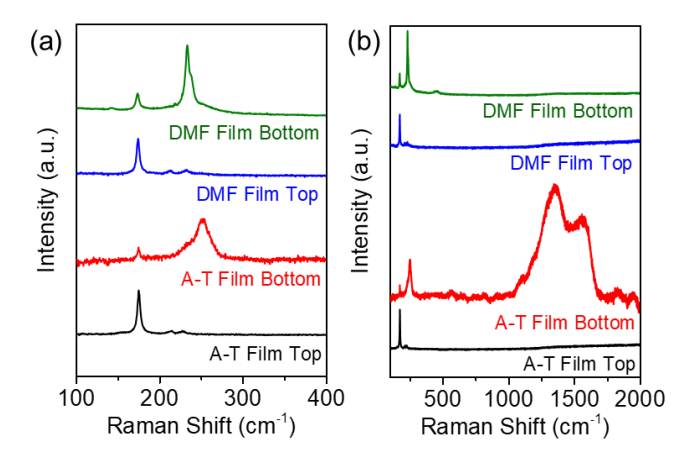
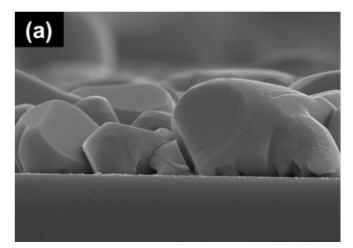


Figure 4. Raman spectra on selenized CIS film fabricated from amine-thiol (A-T) based route and DMF based route from both top and bottom surface of the film. (a) Raman spectra focused near CISe peaks and (b) Full Raman spectra

Unlike the amine-thiol system, another route in the literature using the DMF as a solvent and thiourea as a complexing agent has demonstrated fine-grain free CISe films with a absorber thickness up to 1.2-1.3 microns. This route has claimed to create a carbon-free film which could be a reason for its success with creating fine-grain free films. ²⁹ However, despite the ability to create carbon-free films, the DMF-TU route hasn't reported any absorber above 1.3 µm thickness suggesting the possibility of some additional challenges besides carbon in creating a thicker absorber. To investigate this, two CIS films, one with 1-micron thickness and the other with 2-micron thickness were fabricated using DMF-TU based route and selenized in a TF. Consistent with reports in the literature, the 1-micron thick DMF-TU film indeed formed a fine-grain free morphology (Figure 5a). However, the 2-micron thick DMF-TU film showed the formation

of a secondary fine structured layer at the bottom of the selenized film (Figure 5b). When analyzed under Raman spectroscopy after exfoliation, this layer showed a strong Se peak corresponding to trigonal selenium at around 234 cm⁻¹ instead of amorphous selenium²⁵ as was observed in the case of amine-thiol film (Figure 4a). As both DMF and TU chemicals do not have any C-C bond, it was expected to see a clean spectrum near the graphitic carbon region. However, the fact that Se was retained in the film despite the high processing temperature during selenization, suggests the possible coordination of Se with some undesired species in the solution and formation of a secondary layer in thicker films.



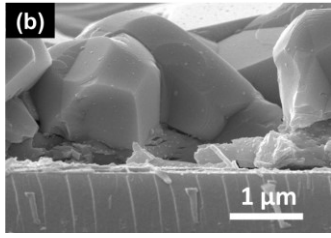


Figure 5. Cross-section SEM images of (a) 1 μ m and (b) 2 μ m thick CISe film fabricated by selenization of DMF based CIS film showing the presence of fine-grain layer in the case of 2 μ m thick film

Finally, when 2 μm thick DMF-TU film was analyzed under SEM-EDS at different spots, it was observed that the bottom of the film (fine-grain region) and the top of the film had different Cu/In and Se/cation ratio suggesting nonuniformity of the elemental distribution in the final film (Figure S5). This was also evident from the STEM-EDS mapping performed on thin lamella obtained from selenized amine-thiol CIS film using a focused ion beam (FIB) technique. This mapping shows the presence of Se, C, and Cu with the absence of indium in the fine-grain layer (Figure 6) which is consistent with previous reports on elemental mapping of CIGSe films, confirming the non-uniformity in elemental distribution across the film thickness. 30,31

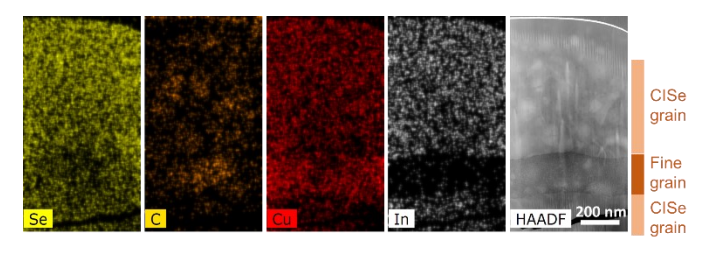


Figure 6. STEM-EDS elemental mapping of thin lamella obtained from selenized CIS film showing elemental non-uniformities between grain and fine-grain layer in the film

The mechanism that is responsible for creating metal non-uniformity and segregating Se-rich material at the bottom of the film could be occurring during the process of selenization. Reports in the literature have shown that the process of sulfide to selenide conversion in the case of CZTS, or even pure metal to metal selenide in the case of CIGS proceeds through the formation of Cu-Se rich liquid phase which starts nucleating copper selenide material. 32–35 The remaining cations then start diffusing towards these nuclei making desired ternary or quaternary selenide materials in the form of grains on the surface of the film that continues to grow towards the bottom (Figure 7a). In this process, especially when the film exceeds a certain thickness, the rate of mass transfer and the reaction rates between copper and indium

chalcogenides could affect the elemental distributions and hence the grain growth in the film. 30,31,36 Based on these results, it is hypothesized that to enable thick film fabrication of CISe/CIGSe absorber, free of any phase/elemental non-uniformities, the precursor film should meet the following two criteria before selenization; 1) the precursor film should be a selenide film instead of a sulfide film which will avoid dissolution of Cu in Se liquid allowing for bulk sintering growth mechanism which should result in uniform elemental distribution throughout the film and 2) the precursor film should be free of any contamination like carbon to avoid segregation of those contaminants in the form of a fine-grain layer. To meet these criteria, Se addition to the precursor film is required which can be achieved in the case of the amine-thiol route as it enables room temperature dissolution of elemental Se and even metal selenides suitable for CISe/CIGSe film fabrication.

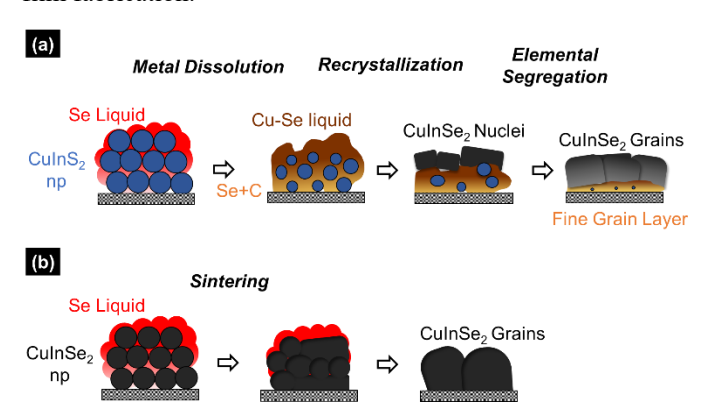


Figure 7. Schematic representation of the CISe grain growth mechanism during selenization for (a) CIS precursor film and (b) CISe precursor film

Se Addition in Precursor Film:

The amine-thiol solvent system can dissolve Se along with metal precursors and such solutions have been used in past for the synthesis of CISSe nanoparticles with different compositions of S and Se.³⁷ Similar solutions were prepared by dissolving Cu₂S and In in BA-EDT solution and adding different quantities of elemental selenium. Se addition to the sulfide ink was performed to get Se/In ratio of 1, 2, and 4 corresponding to 50% of stoichiometric, stoichiometric, and 100% excess Se respectively. Precursor films fabricated from these inks after coating and annealing on hot plate resulted in the formation of sulfoselenide material which was analyzed using Raman spectroscopy and X-ray fluorescence (XRF). All films showed peaks corresponding to both CIS and CISe material with higher Se containing inks showing a higher relative ratio of the CISe/CIS peak in the Raman spectra (Figure S6). Similarly, XRF showed a Se/In ratio of 0.5, 1.4, and 1.8 for the films fabricated from inks having Se/In ratio of 1, 2, and 4 respectively. The 100% excess Se ink appeared to give mostly selenide material, however, due to the use of the excess quantity of elemental Se in the ink, the precursor film exhibited porous morphology caused by loss of volume via free selenium evaporation during the annealing process (Figure 8d).

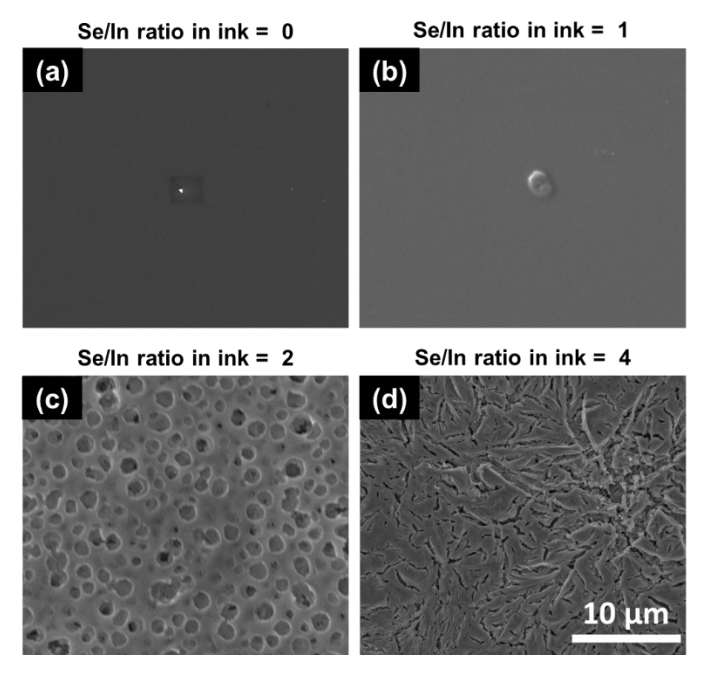


Figure 8. Top-view SEM images of precursor films fabricated using CIS inks containing different Se quantities. (a) 0%, (b) 50% of stoichiometric, (c) stoichiometric, and (d) 100% excess

Such porous precursor films cannot be used for creating a dense absorber layer as it would lead to a possible shunting in the device. While one could dilute the ink to minimize this porosity, using such a dilute ink will require an excessive number of coatings for creating the desired thickness of the film posing difficulty for scale-up. Also, despite using 100% excess Se in the ink (Se/In ratio of 4), the final Se/In ratio in the film was only 1.8 which suggests most of the Se is lost via vaporization during annealing and doesn't get incorporated in the film. The reason for this behavior can be explained based on the Se species found in the solution. It has been shown in previous studies that Se in amine-thiol solution forms polyselenide species which consist of multiple Se atoms sharing a common negative charge.³⁸ This implies that very few Se atoms are completely reduced while most are still present in elemental form lowering the overall reactivity of Se with metal cations. So, to increase the Se quantity in the film, one needs to increase the quantity of completely reduced Se species (Se anions) in the solution. This can be achieved by dissolving metal selenide precursors like Cu₂Se and In₂Se₃ which contain all Se atoms in reduced form instead of a mixture of Cu₂S, In, and elemental Se. To verify the impact of using selenide precursors on selenium incorporation in the film, a metal selenide ink with Cu₂Se and In₂Se₃ was prepared in BA-EDT solution and a precursor film was fabricated by annealing at 300 °C. This ink had an overall Se/In ratio of 2 which was similar to one of the previous inks having stoichiometric Se quantity (i.e. both inks had an equal amount of selenium moles but the different extent of overall Se reduction). However, the XRF data obtained on this film yielded Se/In ratio of 1.8 which is much higher than that of 1.4 obtained previously for the sulfide ink with dissolved Se having Se/In ratio of 2. This result emphasizes the importance of the nature of Se species in the solution and further supports the hypothesis thathaving more Se anions yields higher Se incorporation in the precursor film. To further increase the Se incorporation, 100% excess Se was added to metal selenide ink and a precursor film without any distinct porosity was fabricated. This film showed Se/In ratio of 2.6 with a residual presence of CIS from XRF and Raman spectroscopy (Figure 9). Once the desired elemental composition of precursor film was achieved from the metal selenide precursors, the presence of carbon was also analyzed using Raman spectroscopy. As discussed earlier, the breaking of C-S bond in thiols likely leads to the formation of graphitic carbon in the film. So, if the Se anion is replacing the thiolate and forming metal selenide bond, the metal-S bond in the thiolate will break instead of C-S bond which would allow the thiol molecule to leave the film easily by simple evaporation (Scheme S1). This mechanism is supported by Raman data which shows a decrease in graphitic carbon peak in the precursor film having more selenium concentration (Figure 9). However, another possible route for incorporating Se in the precursor film could be a two-step process where CIS is formed first and then it reacts with elemental Se in the film giving CISe material. In such a process, due to the formation of CIS material in the first step, the carbon content will remain higher. This possible mechanism was confirmed when films were fabricated from an ink having Se/In ratio of 2 at different temperatures. The sudden exposure to higher temperature allowed for quick decomposition of thiolates to sulfides along with rapid evaporation of free Se from the film giving more CIS material and carbon compared to film annealed at a lower temperature which has more Se incorporation and less carbon (Figure S7). The correlation between Se and C, i.e. more selenide material leads to lower carbon is further validated by Raman spectra collected on precursor films fabricated from various ink combinations of Cu, Cu₂S, In, Cu₂Se, In₂Se₃, and Se (Figure S8). Along with graphitic carbon, the CISe ink prepared from selenide precursors and elemental selenium also showed removal of organic carbon at temperature as low as 250 °C which is around 100 °C lower than what was needed for sulfide precursor film, further confirming the importance of Se anion on the removal of organic residue from the film (Figure S9). This film when annealed at 300 °C showed an XRF and Raman spectrum identical to hydrazine based CISSe precursor film implying a formation of superior quality precursor film from a non-hydrazine solution route (Figure S10).

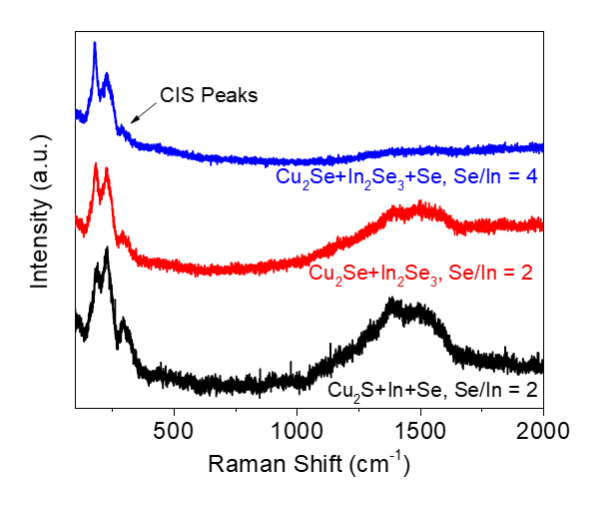


Figure 9. Raman spectra of precursor films fabricated with different inks showing reduction in CIS peak and carbon peak with increasing selenium anion quantity in the solution

Annealing Optimization:

With the successful fabrication of selenide precursor film largely free of detectable impurities, the difference in the growth mechanism for CIS and CISe precursor films fabricated

directly on Mo coated glass substrate was studied by performing a time study during the process of selenization. Both CIS and CISe films were treated with selenium pellets at a temperature of 500 °C for 2 min, 4 min, and 6 min, in a graphite box which was immediately pulled out of the heating zone and allowed to cool down to room temperature. These samples were then analyzed by SEM, XRD, and Raman. The XRD and Raman spectra show a transition of the CIS material to CISe material, and shows formation of larger crystalline domains for both CIS and CISe samples for even the lowest processing time of 2 min (Figure S11). SEM on the other hand reveals more differences in the growth mechanism (Figure 10). As expected, the CIS film shows the formation of grains on the surface of the film at 2 min which is followed by the formation of grains at the back Mo surface (no MoO3 was used in this sample) forming an unsintered fine-grainlike layer in the middle. After 6 min both grain layers continue to grow while maintaining the trilayer morphology. This growth is also observed from top-view SEM images of these films where the average grain size shows an increase with time (Figure S12). On the other hand, CISe precursor film does not show any preferential grain growth on any surface. As previously hypothesized, the film undergoes bulk sintering where the grains keep growing throughout the thickness of the film irrespective of the location. Because of such bulk sintering, the top-view SEM images don't show a drastic change in the grain sizes as a function of time.

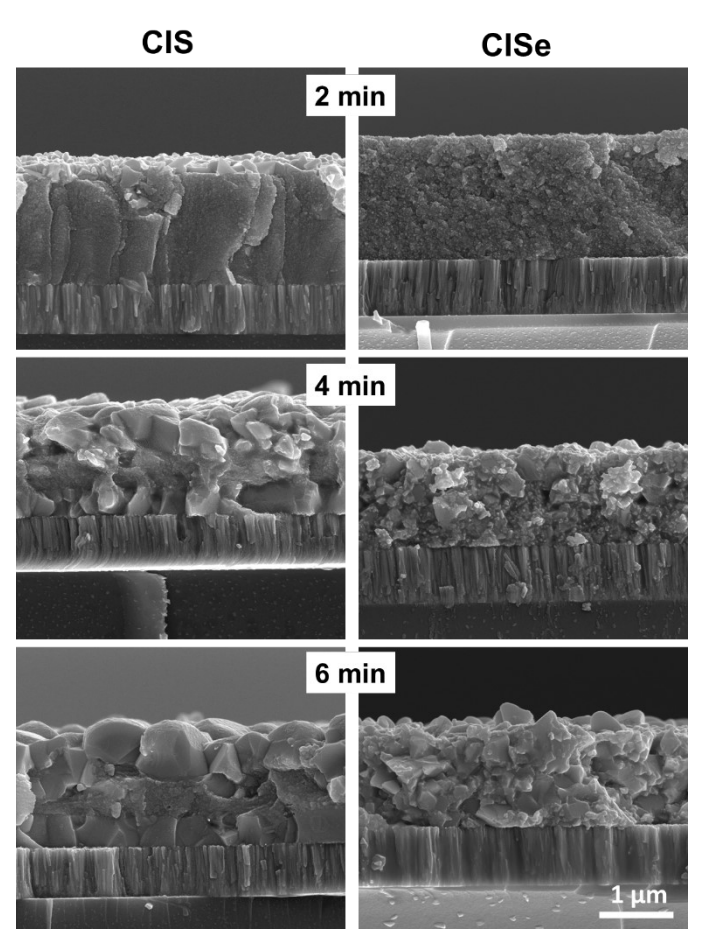


Figure 10. Cross-section SEM images of selenized CIS and CISe precursor films for different time intervals

The modified growth mechanism of surface-independent bulk growth provides a route for growing uniform absorbers irrespective of their thickness. To investigate the thickness independence on film growth, two precursor films were fabricated using CISe precursor inks with a total of 6 layers and 12 layers. These films were then selenized in a tube furnace and analyzed under SEM. As can be seen from the images in Figures 11a and 11b, both films showed fine-grain free morphology making the 12 layer film the first-ever reported 2-micron thick fine-grain free film from any hydrazine-free solution processing routes with uniform grain morphology throughout the film thickness. Similar to CISe film, selenization of gallium containing CIGSe precursor films also create fine-grain free morphologies with certain elemental compositions (Figure 10c). While selenization of CISe precursor films yields significant grain growth, hydrazine-based precursor films have been shown to grow grains with inert atmosphere annealing instead of selenization. This was possible due to the presence of excess chalcogen in the precursor film. As amine-thiol based CISe precursor film showed identical Raman spectrum and composition to that of hydrazine based CISe precursor film, similar behavior of inert atmosphere growth was expected from amine-thiol based CISe precursor films. This was verified by annealing the CISe precursor film in a nitrogen atmosphere rapidly to around 540 °C. The resultant film not only formed a large grain morphology, but due to the lack of vapor phase Se at higher temperatures it also created extremely flat film surfaces (Figure 11d). This morphology is very similar to ones reported in the literature for hydrazine-based films as well as vacuum-based films and have great potential for large-scale manufacturing due to a simple high-temperature inert atmosphere annealing procedure.

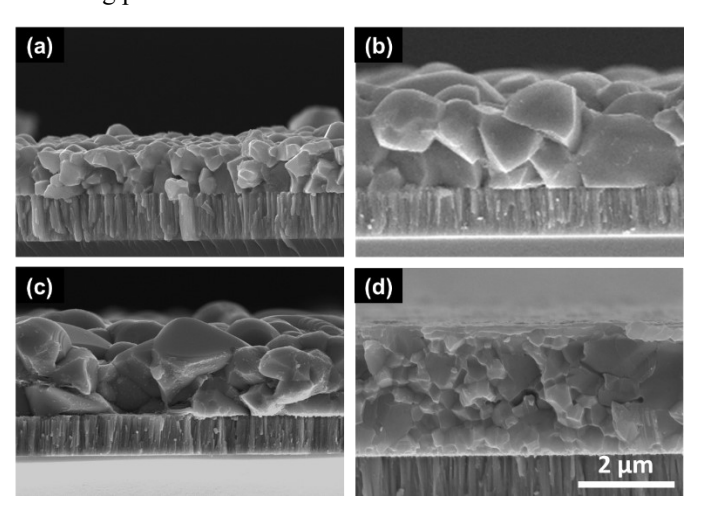


Figure 11. Cross-section SEM images of (a) \sim 1 μ m thick and (b) \sim 2 μ m thick selenized CISe precursor films, (c) \sim 2 μ m thick selenized CIGSe precursor film (Ga/Ga+In=0.1), and (d) \sim 2 μ m thick 540 °C annealed CISe precursor film

Despite the promising film morphology, the optoelectronic properties of the new CISe film are poor compared to a device fabricated from CIS precursor film. The power conversion efficiency observed for this film was only around 3.04%, with Jsc, Voc, and FF of around 20.2 mA/cm², 310 mV, and 48.5% respectively. Comparing the JV data for this device with a device fabricated from CIS precursor film suggests similar dark shunting behavior in both cases (Figure 12a). However, the new CISe device shows a unique light shunting characteristic in reverse bias. It also shows crossover at a much lower voltage which has been previously correlated with defect formation near the CdS interface. ³⁹ Along with JV data, the photoluminescence

of the new CISe material shows almost an order of magnitude lower signal compared to traditionally grown CISe film from sulfide precursor (Figure 12b). These results suggest the possible formation of defects in the bulk and/or near the interface of the newly grown material (also see Figure S13). There are few possible reasons for the formation of defects in this new film; 1) Due to the bulk sintering of the film, any residual carbon impurity which is not getting detected by Raman spectroscopy might be getting trapped between grains instead of getting pushed at the back of the film. This could affect the electron-hole recombination and lower the performance. 2) Due to the absence of any copperselenium liquid which is generally responsible for grain growth at higher temperatures, the bulk sintering might be causing the formation of multiple crystal domains in a grain leading to multiple grain boundaries in the bulk of a microstructure grain observed in SEM. 3) Due to the selenide precursor film, the selenium wetting on the surface at the start of selenization and also during the cooling of the film could be different which could cause different defect concentration profiles in the film. Along with these, one could also correlate the poor device performance to the newly developed selenide precursor inks and the quality of precursor films themselves. However, devices fabricated from hydrazine based precursor films under similar selenization conditions also produced poor performance when replicated for this work, suggesting a possible issue with the high temperature annealing step (Figure S14). As previous literature on hydrazine based films has highlighted the importance of annealing steps on device performance and has demonstrated much higher performance with detailed optimization, similar work is required with this new hydrazine-free CISe precursor film, to realize the high efficiency devices.³⁹ Techniques like KPFM, CV, Admittance, PL, TRPL, JVT are crucial in further investigation of defect behavior in these films.

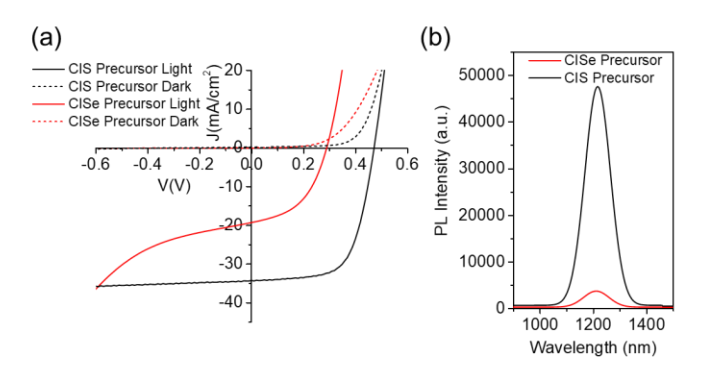


Figure 12. (a) JV data and (b) PL data on selenized CIS and CISe precursor films

Conclusion:

In conclusion, we showed an impact of the fine-grain layer on the performance of CISe/CIGSe devices. By manipulating the location of the fine-grain layer in the film structure through deposition of thin MoO₃ layer, CISe and CIGSe device efficiencies of 12.9% and 14.1% were achieved for uniform composition films respectively. Analysis performed on fine-grain layer suggested Se and carbon as the primary content along with some other cations with non-uniform distributions. Similar to amine-thiol solution route, even the DMF-TU based route showed the formation of a Se rich fine-grain layer for thicker films which suggested CIS precursor film as a possible cause of

fine-grain layer formation. By adding Se in amine-thiol based inks, the reduction of sulfide content, as well as carbon content, was observed which was then optimized by replacing metal and metal sulfides with metal selenides to get complete absence of detectable carbon from the film and achieve precursor film identical to high efficiency hydrazine based routes from the literature. With modified precursor film from sulfide to selenide material, the growth mechanism was changed to bulk growth resulting in a fine-grain free film with thickness as high as 2micron. Due to the presence of selenium in precursor film, grain growth in the absence of vapor phase selenium was also demonstrated by simply annealing the film in an inert atmosphere at higher temperatures which resulted in grain growth with the added benefit of particularly flat surface. While the grain growth modification indeed resulted in film morphologies similar to hydrazine based routes, further high temperature annealing optimization along with defect characterization is required to obtain low defect and high performing CISe/CIGSe films.

Acknowledgment:

The authors would like to acknowledge the funding support provided by the National Science Foundation under Grants 1534691-DMR (DMREF), 1735282-NRT (SFEWS), and 1855882 (INFEWS). The research was carried out in part at the Center for Functional Nanomaterials, Brookhaven National Laboratory, which is supported by the U.S. Department of Energy, Office of Basic Energy Sciences, under Contract No. DE-SC0012704.

References:

- 1. Nakamura, M., Yamaguchi, K., Kimoto, Y., Yasaki, Y., Kato, T. & Sugimoto, H. Cd-free Cu(In,Ga)(Se,S)₂ thin-film solar cell with a new world record efficacy of 23.35%. in *46th IEEE PVSC* (2019).
- 2. Friedlmeier, T. M., Jackson, P., Bauer, A., Hariskos, D., Kiowski, O., Menner, R., Wuerz, R. & Powalla, M. High-efficiency Cu(In,Ga)Se₂ solar cells. *Thin Solid Films* **633**, 13–17 (2017).
- 3. Lee, T. D. & Ebong, A. U. A review of thin film solar cell technologies and challenges. *Renew. Sustain. Energy Rev.* **70**, 1286–1297 (2017).
- 4. Zhang, T., Yang, Y., Liu, D., Tse, S. C., Cao, W., Feng, Z., Chen, S. & Qian, L. High efficiency solution-processed thin-film Cu(In,Ga)(Se,S)₂ solar cells. *Energy Environ. Sci.* **9**, 3674–3681 (2016).
- 5. Guo, Q., Ford, G. M., Hillhouse, H. W. & Agrawal, R. Sulfide Nanocrystal Inks for Dense Cu(In_{1-x}Ga_x)(S_{1-y}Se_y)₂ Absorber Films and Their Photovoltaic Performance. *Nano Lett.* **9**, 3060–3065 (2009).
- 6. Mitzi, D. B., Yuan, M., Liu, W., Kellock, A. J., Jay Chey, S., Deline, V. & Schrott, A. G. A high-efficiency solution-deposited thin-film photovoltaic device. *Adv. Mater.* **20**, 3657–3662 (2008).
- 7. Suresh, S. & Uhl, A. R. Present Status of Solution-Processing Routes for Cu(In,Ga)(S,Se)₂ Solar Cell Absorbers. *Adv. Energy Mater.* **11**, (2021).

- 8. Zhao, Y., Yuan, S., Chang, Q., Zhou, Z., Kou, D., Zhou, W., Qi, Y. & Wu, S. Controllable Formation of Ordered Vacancy Compound for High Efficiency Solution Processed Cu(In,Ga)Se₂ Solar Cells. *Adv. Funct. Mater.* **2007928**, 1–10 (2020).
- 9. Fan, Q., Tian, Q., Wang, H., Zhao, F., Kong, J. & Wu, S. Regulating the starting location of front-gradient enabled highly efficient Cu(In,Ga)Se₂ solar cells *via* a facile thiol–amine solution approach. *J. Mater. Chem. A* **6**, 4095–4101 (2018).
- Zhao, Y., Yuan, S., Kou, D., Zhou, Z., Wang, X., Xiao, H., Deng, Y., Cui, C., Chang, Q. & Wu, S. High Efficiency CIGS Solar Cells by Bulk Defect Passivation through Ag Substituting Strategy. ACS Appl. Mater. Interfaces 12, 12717–12726 (2020).
- Yuan, S., Wang, X., Zhao, Y., Chang, Q., Xu, Z., Kong, J. & Wu, S. Solution Processed Cu(In,Ga)(S,Se)₂ Solar Cells with 15.25% Efficiency by Surface Sulfurization. ACS Appl. Energy Mater. 3, 6785–6792 (2020).
- 12. McLeod, S. M., Hages, C. J., Carter, N. J. & Agrawal, R. Synthesis and characterization of 15% efficient CIGSSe solar cells from nanoparticle inks. *Prog. Photovoltaics Res. Appl.* **23**, 1550–1556 (2015).
- Park, G. S., Chu, V. Ben, Kim, B. W., Kim, D. W., Oh, H. S., Hwang, Y. J. & Min, B. K. Achieving 14.4% Alcohol-Based Solution-Processed Cu(In,Ga)(S,Se)₂ Thin Film Solar Cell through Interface Engineering. ACS Appl. Mater. Interfaces 10, 9894–9899 (2018).
- 14. Uhl, A. R., Katahara, J. K. & Hillhouse, H. W. Molecular-ink route to 13.0% efficient low-bandgap CuIn(S,Se)₂ and 14.7% efficient Cu(In,Ga)(S,Se)₂ solar cells. *Energy Environ. Sci.* **9**, 130–134 (2016).
- Jiang, J., Giridharagopal, R., Jedlicka, E., Sun, K., Yu, S., Wu, S., Gong, Y., Yan, W., Ginger, D. S., Green, M. A., Hao, X., Huang, W. & Xin, H. Highly efficient copper-rich chalcopyrite solar cells from DMF molecular solution. *Nano Energy* 69, 104438 (2020).
- Guo, Q., Ford, G. M., Agrawal, R. & Hillhouse, H. W. Ink formulation and low-temperature incorporation of sodium to yield 12% efficient Cu(In,Ga)(S,Se)₂ solar cells from sulfide nanocrystal inks. *Prog. Photovoltaics Res. Appl.* 21, 64–71 (2013).
- Ellis, R. G., Turnley, J. W., Rokke, D. J., Fields, J. P., Alruqobah, E. H., Deshmukh, S. D., Kisslinger, K. & Agrawal, R. Hybrid Ligand Exchange of Cu(In,Ga)S₂ Nanoparticles for Carbon Impurity Removal in Solution-Processed Photovoltaics. *Chem. Mater.* 32, 5091–5103 (2020).
- Zhao, D., Fan, Q., Tian, Q., Zhou, Z., Meng, Y.-N., Kou, D.-X., Zhou, W.-H. & Wu, S. Eliminating fine-grained layers in Cu(In,Ga)(S,Se)₂ thin films for solution-processed high efficiency solar cells. *J. Mater. Chem. A* 4, 13476–13481 (2016).
- 19. Zhao, X., Lu, M., Koeper, M. J. & Agrawal, R. Solution-

- processed sulfur depleted Cu(In, Ga)Se₂ solar cells synthesized from a monoamine–dithiol solvent mixture. *J. Mater. Chem. A* **4**, 7390–7397 (2016).
- Yu, Q., Shi, J., Guo, L., Duan, B., Luo, Y., Wu, H., Li,
 D. & Meng, Q. Eliminating multi-layer crystallization of Cu₂ZnSn(S,Se)₄ absorber by controlling back interface reaction. *Nano Energy* 76, 105042 (2020).
- 21. Ranjbar, S., Brammertz, G., Vermang, B., Hadipour, A., Cong, S., Suganuma, K., Schnabel, T., Meuris, M., da Cunha, A. F. & Poortmans, J. Improvement of kesterite solar cell performance by solution synthesized MoO₃ interfacial layer. *Phys. Status Solidi Appl. Mater. Sci.* 214, 1–6 (2017).
- 22. Liu, L., Lau, T. K., Zhi, Z., Huang, L., Wang, S. & Xiao, X. Modification of Mo Back Contact with MoO_{3-x} Layer and its Effect to Enhance the Performance of Cu₂ZnSnS₄ Solar Cells. *Sol. RRL* **2**, 1–10 (2018).
- 23. Schnabel, T. & Ahlswede, E. On the interface between kesterite absorber and Mo back contact and its impact on solution-processed thin-film solar cells. *Sol. Energy Mater. Sol. Cells* **159**, 290–295 (2017).
- 24. He, Z., Liu, Y., Lin, S., Shi, S., Sun, S., Pang, J., Zhou, Z., Sun, Y. & Liu, W. Energy Band Alignment in Molybdenum Oxide/Cu(In,Ga)Se₂ Interface for High-Efficiency Ultrathin Cu(In,Ga)Se₂ Solar Cells from Low-Temperature Growth. *ACS Appl. Energy Mater.* 3, 3408–3414 (2020).
- Lucovsky, G., Mooradian, A., Taylor, W., Wright, G. B. & Keezer, R. C. Identification of the Fundamental Vibrational Modes Of Trigonal, Monoclinic and Amorphous Selenium. *Solid State Commun.* 5, 113–117 (1967).
- 26. TUINSTRA F & KOENIG JL. Raman Spectrum of Graphite. *J. Chem. Phys.* **53**, 1126–1130 (1970).
- Canado, L. G., Takai, K., Enoki, T., Endo, M., Kim, Y. A., Mizusaki, H., Jorio, A., Coelho, L. N., Magalhães-Paniago, R. & Pimenta, M. A. General equation for the determination of the crystallite size la of nanographite by Raman spectroscopy. *Appl. Phys. Lett.* 88, 1–4 (2006).
- Zhao, X., Deshmukh, S. D., Rokke, D. J., Zhang, G., Wu, Z., Miller, J. T. & Agrawal, R. Investigating Chemistry of Metal Dissolution in Amine–Thiol Mixtures and Exploiting It toward Benign Ink Formulation for Metal Chalcogenide Thin Films. *Chem. Mater.* 31, 5674–5682 (2019).
- Uhl, A. R., Rajagopal, A., Clark, J. A., Murray, A., Feurer, T., Buecheler, S., Jen, A. K. Y. & Hillhouse, H. W. Solution-Processed Low-Bandgap CuIn(S,Se)₂
 Absorbers for High-Efficiency Single-Junction and Monolithic Chalcopyrite-Perovskite Tandem Solar Cells. *Adv. Energy Mater.* 8, 1–8 (2018).
- 30. Rehan, S., Kim, K. Y., Han, J., Eo, Y. J., Gwak, J., Ahn, S. K., Yun, J. H., Yoon, K. H., Cho, A. & Ahn, S. J. Carbon-Impurity Affected Depth Elemental Distribution

- in Solution-Processed Inorganic Thin Films for Solar Cell Application. *ACS Appl. Mater. Interfaces* **8**, 5261–5272 (2016).
- 31. Uhl, A. R., Fuchs, P., Rieger, A., Pianezzi, F., Sutter-Fella, C. M., Kranz, L., Keller, D., Hagendorfer, H., Romanyuk, Y. E., LaMattina, F., Yoon, S., Karvonen, L., Magorian-Friedlmeier, T., Ahlswede, E., VanGenechten, D., Stassin, F. & Tiwari, A. N. Liquid-selenium-enhanced grain growth of nanoparticle precursor layers for CuInSe 2 solar cell absorbers. *Prog. Photovoltaics Res. Appl.* 23, 1110–1119 (2015).
- Hages, C. J., Koeper, M. J., Miskin, C. K., Brew, K. W. & Agrawal, R. Controlled grain growth for high performance nanoparticle-based kesterite solar cells. *Chem. Mater.* 28, 7703–7714 (2016).
- 33. Kim, W. K., Payzant, E. A., Yoon, S. & Anderson, T. J. In situ investigation on selenization kinetics of Cu-In precursor using time-resolved, high temperature X-ray diffraction. *J. Cryst. Growth* **294**, 231–235 (2006).
- Mainz, R., Walker, B. C., Schmidt, S. S., Zander, O., Weber, A., Rodriguez-Alvarez, H., Just, J., Klaus, M., Agrawal, R. & Unold, T. Real-time observation of Cu₂ZnSn(S,Se)₄ solar cell absorber layer formation from nanoparticle precursors. *Phys. Chem. Chem. Phys.* (2013).
- 35. Carter, N. J., Mainz, R., Walker, B. C., Hages, C. J., Just, J., Klaus, M., Schmidt, S. S., Weber, A., Yang, W. C. D., Zander, O., Stach, E. A., Unold, T. & Agrawal, R. The role of interparticle heterogeneities in the selenization pathway of Cu-Zn-Sn-S nanoparticle thin films: a real-time study. *J. Mater. Chem. C* (2015).
- 36. Ahn, S., Choi, Y. J., Kim, K., Eo, Y. J., Cho, A., Gwak, J., Yun, J. H., Shin, K., Ahn, S. K. & Yoon, K. Amorphous Cu-In-S nanoparticles as precursors for CuInSe₂ thin-film solar cells with a high efficiency. *ChemSusChem* 6, 1282–1287 (2013).
- Deshmukh, S. D., Ellis, R. G., Sutandar, D. S., Rokke,
 D. J. & Agrawal, R. Versatile Colloidal Syntheses of
 Metal Chalcogenide Nanoparticles from Elemental
 Precursors Using Amine-Thiol Chemistry. *Chem. Mater.* 31, 9087–9097 (2019).
- 38. Deshmukh, S. D., Easterling, L. F., Manheim, J. M., LiBretto, N. J., Weideman, K. G., Miller, J. T., Kenttämaa, H. I. & Agrawal, R. Analyzing and Tuning the Chalcogen–Amine–Thiol Complexes for Tailoring of Chalcogenide Syntheses. *Inorg. Chem.* **59**, 8240–8250 (2020).
- 39. Cao, Q., Gunawan, O., Copel, M., Reuter, K. B., Chey, S. J., Deline, V. R. & Mitzi, D. B. Defects in Cu(In,Ga)Se₂ chalcopyrite semiconductors: A comparative study of material properties, defect states, and photovoltaic performance. *Adv. Energy Mater.* 1, 845–853 (2011).

Table of Content Graphic:

